Solvent-free synthesis and hydrophobization of biobased epoxy coatings for anti-icing and anticorrosion applications

Bellido-Aguilar, Daniel Angel; Zheng, Shunli; Huang, Yinjuan; Zeng, Xianting; Zhang, Qichun; Chen, Zhong

2019

Bellido-Aguilar, D. A., Zheng, S., Huang, Y., Zeng, X., Zhang, Q. & Chen, Z. (2019). Solvent-free synthesis and hydrophobization of biobased epoxy coatings for anti-icing and anticorrosion applications. ACS Sustainable Chemistry and Engineering, 7(23), 19131-19141. https://dx.doi.org/10.1021/acssuschemeng.9b05091

https://hdl.handle.net/10356/150809

https://doi.org/10.1021/acssuschemeng.9b05091

Solvent-free synthesis and hydrophobization of bio-based epoxy coatings for anti-icing and anticorrosion applications

Daniel Angel Bellido-Aguilar[a], *Shunli Zheng*[a], *Yinjuan Huang*[a], *Xianting Zeng*[b], *Qichun Zhang*[a], *Zhong Chen*[a,*]

[a] School of Materials Science and Engineering, Nanyang Technological University, 50 Nanyang Avenue, 639798, Singapore

[b] Singapore Institute of Manufacturing Technology, 2 Fusionopolis Way, Singapore 138634

*E-mail: ASZChen@ntu.edu.sg

ABSTRACT

Epoxy resins are widely commercialized in the market because of their important applications such as adhesives, protective and decorative coatings. However, their usages have brought in negative impacts on the environment since approximately 70% of the epoxy resins are prepared from toxic petroleum-based precursor bisphenol. Great effort has been made on the use of bio-based compounds to create an environmentally-friendly epoxy resin industry. In this research, fully bio-based epoxy coatings were prepared from cardanol-derived resins with furfurylamine (FA) or 1,8-Diamino-p-menthane (DAPM) as the curing agent without the use of any solvent. Hydrophobization was realized by the addition of a fluorine-free additive, polydimethylsiloxane (PDMS). The thermal-mechanical and wettability properties of the coatings exhibited a strong dependency on the type of epoxy resin and curing agent. The coatings were also assessed for their anti-icing and anticorrosion performances. The fully bio-based NC514-DAPM coating showed a very low ice adhesion strength at 55.0 ± 5.2 kPa. It also showed good anticorrosive properties as demonstrated in

its high corrosion potential and low corrosion current. Hydrophobization by PDMS was able to further reduce the ice adhesion strength of the fully bio-based coatings by 32-38%, however, its effect on the anticorrosion remains inconclusive due to the varying thicknesses of the coatings.

KEYWORDS: cardanol; hydrophobic; corrosion; ice accretion; furfurylamine.

INTRODUCTION

Epoxy resins are well established in the market due to their various applications such as adhesives, coatings, and electronic packing materials [1, 2]. The most important and widely used epoxy resin is diglycidyl ether of Bisphenol A (DGEBA), which represents approximately 75% of the commercial epoxy resins [3, 4]. However, Bisphenol A (BA), the precursor of DGEBA, is a compound obtained from petroleum sources. Therefore, the current epoxy resin industry is greatly lacking of sustainability since it relies on BA.

An alternative to overcome the dependency on DGEBA is the preparation of epoxy resins from biomass compounds. In recent years, epoxy resins have been prepared from different kinds of bio-based sources such as vegetable oils [5, 6], saccharides [7, 8] and natural phenolic compounds [9, 10]. One of these bio-based phenolic compounds is cardanol, which is extracted from the liquid of the cashew nutshell [11]. For instance, Jaillet et al.[12] studied the mechanical and thermal properties of bulk thermosets based on cardanol. Kanehashi et al. prepared and characterized the properties of cardanol-based epoxy coatings but no specific applications of the coatings were studied [13]. Moreover, cardanol resins have been used in the synthesis of thermosets from epoxy blends [14, 15] and as toughening in epoxy polymers [16-18].

The preparation of hydrophobic cardanol epoxy polymers using ionic liquids has been reported recently. However, there were no evaluations of their anti-icing and anticorrosion performances [19]. On the other hand, studies on the corrosion protection of cardanol epoxy coatings have been carried out [20, 21] using non-bio-based curing agents. To increase the bio content of the coatings, this research focuses on the study of anticorrosion and anti-icing properties of hydrophobic cardanol epoxy coatings using bio-based curing agents. In the past years, there is an increasing research activity in preparing hydrophobic coatings using bio-based epoxies [22-25], however, the bio content of these coatings is limited by the non-bio-based curing agent. To the best of our knowledge, there have been very few reports on hydrophobic thermosets using bio-based epoxy resins and bio-based curing agents [26-28].

In this work, two types of bio-based curing agents were studied, *viz.*, furfurylamine (FA) and 1,8-Diamino-p-menthane (DAPM). FA is a derivative of furfural, obtained from lignocellulosic biomass [29]. Despite the studies of FA as a curing agent since 1992 [30], attention has been only paid to its use for the preparation of polybenzoxazines [31-34]. There has been no report on the use of FA solely as a curing agent for the preparation of epoxy coatings. On the other hand, DAPM is a derivative from the monoterpene limonene [35], and its use as a curing agent for the synthesis of epoxy thermosets is rare [36]. Thus, in the current study, we will investigate the influence of the bio-based curing agents FA and DAPM on the anticorrosion and anti-icing performances of cardanol-epoxy coatings. Effect of a hydrophobic additive, polydimethylsiloxane, on the coating performances has also been evaluated.

EXPERIMENTAL SECTION

Materials

Cardanol epoxy resins NC-547 and NC-514S (abbreviated as NC-514) were obtained from Cardolite. FA, DAPM (85%, mixture of cis & trans isomers) and polydimethylsiloxane, bis(3-aminopropyl) terminated (abbreviate as PDMS; average M_n ~2500) were obtained from Sigma Aldrich. All chemicals were used as received without any further purification. Figure 1 shows the molecular structure of the bio-based compounds and PDMS. Among many available hydrophobic additives, we choose PDMS because it is cheaper and non-toxic in comparison with the fluorinated hydrophobic additives.

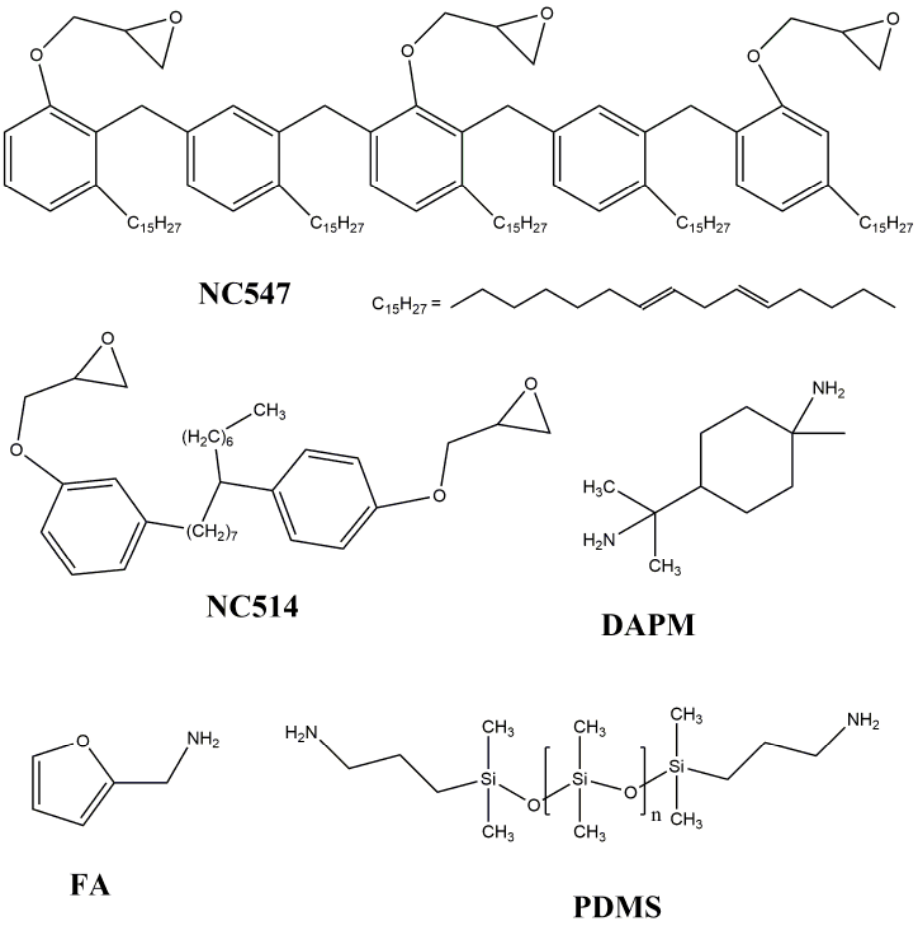

Figure 1. Molecular structures of the bio-based epoxies (NC547, N514), bio-based curing agents (FA, DAPM) and PDMS.

Synthesis of the bio-based polymer coatings

Two sets of samples were prepared. This first set of samples was prepared from the combination of an epoxy resin and a curing agent: NC547-FA, NC547-DAPM and NC514-DAPM. The second set of samples was prepared by adding in 10% (w/w) PDMS as hydrophobic additive into the first set of samples. The samples with PDMS were denoted as NC547-FA-PDMS, NC547-DAPM-PDMS and NC514-DAPM-PDMS, respectively.

To avoid the release of volatile organic compounds during coating processing, this study did not use of any solvent. The epoxy resin and the curing agent were mixed with a spatula in a stoichiometry ratio based on the epoxy equivalent weight (EEW) and amine hydrogen equivalent weight (AHEW). The EEWs of the resins were obtained by titration and AHEWs of the curing agents were calculated theoretically. For the preparation of the second set of samples, PDMS was mixed with the mixture of the epoxy resin and curing agent. The mixture was then degassed with the aid of an ultrasonicator. Thick coatings and thin coatings were prepared by drop-casting method on Fe substrates. Curing was carried out at 180°C for 5.5 hours in a conventional oven. Thin coatings with thickness around 3-9 µm were used exclusively in electrochemical analysis, while thick coatings (thickness higher than 30 µm) were employed for the rest characterizations and performance evaluations.

Characterization

The EEWs of the NC-547 and NC-514 were measured by titration following a standard method (ASTM D1652).

Thermogravimetric Analysis (TGA) of the samples were carried out in a TGA Q500 (TA Instruments). The samples with weights of approximately 10 mg were placed in alumina crucibles and heated from room temperature to 600°C at 10°C/min under nitrogen flow (60 mL/min). Three measurements were performed for each sample and the data was analyzed by the software TA Universal Analysis.

A DSC Discovery (TA Instruments) was used for studying the curing kinetics of the epoxy resins. The samples were analyzed immediately after the preparation of the mixture. The samples with weight around 1- 4 mg were encapsulated in hermetic pans and heated from 25°C to 300°C under nitrogen flow (50 mL/min). Four different heating rates (5, 10, 15 and 20 °C/min) were used for the analyses and at least two measurements were carried out for each heating rate.

The measurement of the viscosity of the all formulations was carried on a rheometer Discovery HR-3 (TA Instruments) using a parallel-plate geometry with a gap of 500 µm at 25°C.

The identification of the functional groups of the coatings were performed by Fourier-transform infrared (FTIR) spectroscopy. Coatings were tested in a FTIR MIR/NIR Frontier (Perkin Elmer) in an attenuated total reflectance (ATR) mode. The analyses were conducted in a wavelength range of 4000-600 cm^{-1}, with 32 scan accumulations and with a resolution of 4 cm^{-1}. The baselines of the spectra were corrected by the software Spectrum (PerkinElmer).

Static contact angles of 5 µL droplets of DI water, ethylene glycol and glycerol deposited on the coatings were measured in an OCA 20 goniometer (Dataphysics). The surface energy

was calculated using the Neumann`s equation of state [37] as provided in the software SCA 20 (Dataphysics). The water contact angle hysteresis was measured by the sessile drop method in which the droplet volume was increased and reduced by 5 µL at a rate of 1 µL/s.

Dynamic mechanical analysis (DMA) was carried out in a DMA Q800 (TA Instruments) with a deformation amplitude of 4 µm at 1 Hz. Due to the different stiffness, NC547-based coatings were tested in compression mode while NC514-based coatings were evaluated in tension mode. The pairs of polymers, NC547-FA and NC547-FA-PDMS, NC514-DAPM and NC514-DAPM-PDMS, and NC547-DAPM and NC547-DAPM-PDMS, were heated from -30°C to 150°C, -30°C to 100°C, and -20°C to 150°C, respectively. Three samples were tested for each composition.

A surface profiler (KLA Tencor) was used to determine the thickness of the coatings. The stylus of the profilometer runs across uncoated region to the coated region, and the difference in height is the coating thickness.

Atomic force microscopy (AFM) was carried out in an AFM Cypher S (Asylum Research) in tapping mode using a soft cantilever. Area of 20 × 20 μm^2 was scanned in three different locations of each coating.

The ice adhesion of the samples was evaluated by measuring the shear strength to remove an ice block formed on the surface of coating. The set up used for these measurements was the same as that described before[38] . The ice block was formed by placing a cap filled with water on the surface the coatings at -20°C for 24 hours in an ice chamber (Cincinnati Sub-Zero environmental chambers, USA). An adhesion tester placed inside the ice chamber was used to measure the shear force necessary to remove the ice. The force was normalized by the area

of the ice block and reported in Pa. The reported ice adhesion for each sample was the average of at least 3 measurements.

Electrochemical analysis was carried out in three-electrode cell in an electrochemical workstation (CHI 660d, Shanghai Chenhua Instrument Corporation). The tests were conducted in a 3.5% NaCl solution using Ag/AgCl and Pt as the reference and counter electrodes, respectively. The coatings with area of 1 cm^2 were immersed in the electrolyte for 1 hour before the experiment.

RESULTS AND DISCUSSION

Curing of coatings

The EEWs of NC547 and NC514 found by the titration methodology (ASTM D1652) were 786 g/eq and 450 g/eq, respectively. These values were within the range of the EEWs of NC547 (550-850) and NC514 (425-575) provided by the supplier.

The main functional groups of the precursors were identified by FTIR (Figure 2a). The presence of the amino groups of the bio-based curing agents, FA and DAPM, was confirmed by the appearance of the absorption band at ~1600 cm^{-1}. The ether group of FA was also identified and assigned to the absorption band at 1148 cm^{-1}. The epoxy rings of NC547 and NC514 were distinguished and associated to the stretching absorption band at 910 cm^{-1} [13]. In the hydrophobic additive, PDMS, two kinds of vibration (stretching and bending) of the bond C-H were identified and associated to the bands at 2963 and 1258 cm^{-1}, respectively [39]. The absorption bands of Si-O and Si-C were also found at 1011 and 789 cm^{-1}, respectively.

ATR-FTIR analysis was also carried out on the surface of the bio-based coatings (Figure 2 b-d). Two main aspects can be highlighted from the FTIR spectra. First, all the coatings are

characterized by the presence of carbonyl groups after curing. The origin of the carbonyl groups can be attributed to the thermal oxidation due to the presence of oxygen [13, 40]. Second, the conversion of the epoxy groups is different for each sample and depends on the kind of epoxy resin. It is evident that the epoxy groups still remained after the heat treatment in the samples NC547-FA, NC547-FA-PDMS, NC547-DAPM and NC547-DAPM-PDMS (Figure 2b and 2c, inset). However, epoxy groups were totally consumed during the curing reaction in the preparation of the samples NC514-DAPM and NC514-DAPM-PDMS (Figure 2d, inset). A possible explanation for the different degree of curing in the NC514-based coatings and NC547-based coatings is the viscosity of the epoxy resins. Based on the product information from the supplier, the viscosity of NC547 ranges from 20 to 50 Pa·s, while the viscosity of NC514 varies from 10 to 35 Pa·s. The differences in viscosity between the NC547-based and NC514-based formulations are shown in Figure S1. The results showed that in the Newtonian region the viscosity of NC547-based formulations varied from 58 to 225 Pa·s, while the viscosity of NC514-based formulations changed from 2.4 to 3.5 Pa·s. Since no solvent was used in the preparation of the coatings, the high viscosity of NC547 might have prevented the full reaction between epoxy and amino groups during the thermal treatment.

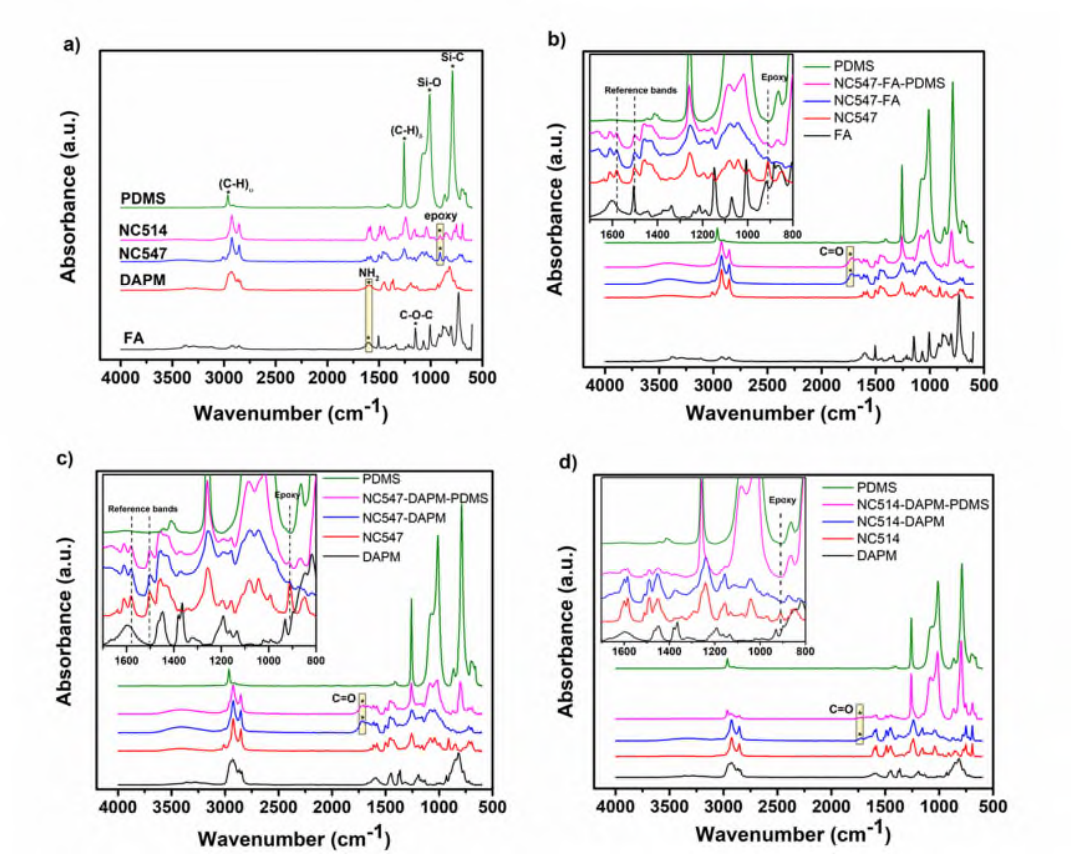

Figure 2. FTIR spectra of the a) precursors, b) coatings NC547-FA and NC547-FA-PDMS, c) coatings NC547-DAPM and NC547-DAPM-PDMS, and d) coatings NC514-DAPM and NC514-DAPM-PDMS.

The degree of epoxy conversion of the coatings (α_{coat}) is given in equation 1 [41]:

$$\alpha_{coat} = \frac{I_{er} - I_{coat}}{I_{er}} \qquad (1)$$

where I_{er} and I_{coat} are the normalized intensity of the epoxy absorption peak (910 cm^{-1}) in the epoxy resin and the coating, respectively. For comparison, two reference bands at 1581 and 1503 cm^{-1} were used for the normalization. These two peaks can be assigned to the

stretching vibrations of aromatic carbon-carbon bonds that remain stable and unreacted during the curing process[42]. The 1503 cm^{-1} reference band works well with NC547-DAPM samples since there is no interference with other bands from DAPM or PDMS. Similarly, the 1581 cm^{-1} reference band works well with NC547-FA samples because of the non-interference with other bands of FA or PDMS. As shown in Table 1, when comparing samples without the hydrophobic additive PDMS, the degrees of epoxy conversion of the samples NC547-FA and NC547-DAPM were similar regardless of the chosen reference band. A similar effect in the epoxy conversion was also found in the samples with PDMS. Moreover, the epoxy conversion was higher in the coatings containing PDMS than the ones without. Due to its low viscosity (1.96 Pa·s), PDMS may have acted as a plasticizer and, thus, promoting the reaction between the amino and epoxy groups. Another possibility is that PDMS reacted with the epoxy groups, therefore, increasing the epoxy conversion rate. More insights into the roles by PDMS will be discussed later based on DSC results.

Table 1. Various properties of the bio-based coatings.

Sample	Epoxy conversion (%) Reference band 1581 cm^{-1}	Epoxy conversion (%) Reference band 1503 cm^{-1}	E_a (kJ/mol Epoxy)	WCA (°)	Surface energy (mJ/m^2)
NC547-FA	65	51	30.57 (±2.95)	83.51 (±1.44)	31.54 (±1.46)
NC547-DAPM	69	54	45.41 (±4.78)	75.68 (±3.53)	32.35 (±3.29)
NC514-DAPM	~100	~100	46.43 (±1.93)	95.43 (±1.04)	26.14 (±0.49)
NC547-FA-PDMS	80	73	28.47 (±2.73)	97.22 (±1.38)	21.20 (±2.06)
NC547-DAPM-PDMS	83	76	60.93 (±3.65)	100.19 (±1.74)	20.34 (±1.40)
NC514-DAPM-PDMS	~100	~100	43.14 (±0.93)	114.00 (±0.63)	13.25 (±1.01)

Further analyses of the curing reactions were carried out through the calculation of the activation energies by using the Kissinger equation [43-45]:

$$\frac{d\ln\left(q/T_p^2\right)}{d\left(1/T_p^2\right)} = -\frac{E_a}{R} \qquad (2)$$

where q, T_p, E_a and R are, respectively, the heating rate, peak temperature, energy of activation and the universal gas constant. It was found that some of the DSC curves of reactions showed two exothermic peaks (Figure 3). The two peaks can be attributed to two different reactions: the reaction between a primary amino group and the epoxy group, and the reaction between a secondary amino group and the epoxy group [36]. Therefore, reaction curves with two peaks were deconvoluted (inset, Figure 3) and the first peak was used for the calculation of activation energies. Figure 4a shows the Kissinger plots and Table 1 lists the E_a values. When comparing samples without PDMS, the E_a values of samples cured with FA and DAPM were ~30 kJ/mol and ~45 kJ/mol, respectively. It is noticeable that the E_a values of samples containing PDMS were the same as those without PDMS for each kind of curing agent. One exception was the E_a of NC547-DAPM-PDMS that showed an increased activation energy (57.75 kJ/mol) in comparison with that of NC547-DAPM (45.41 kJ/mol).

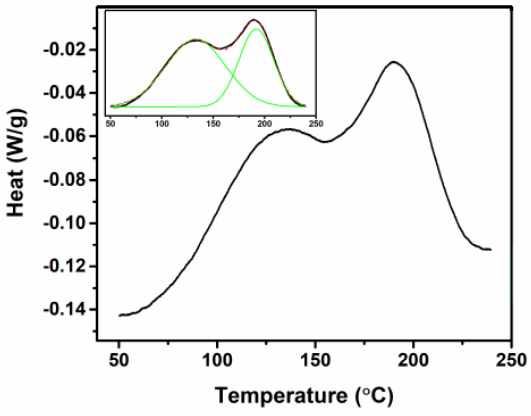

Figure 3. Typical exothermic curve of the reaction between amino and epoxy groups. The inset shows the deconvolution of the curve. Green curves are the resulted Gaussian curves; dash read curve (largely overlaps with the black solid line) is the sum of the green Gaussian curves.

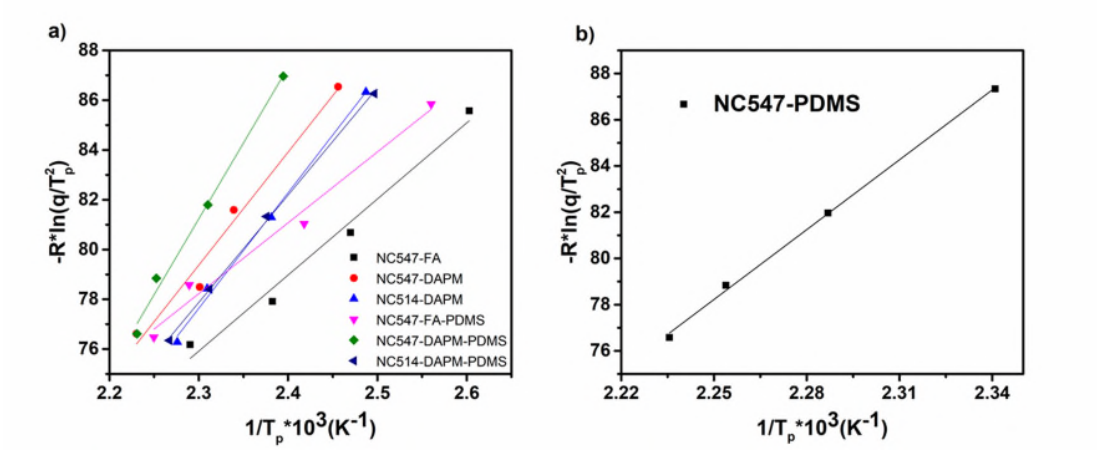

Figure 4. Kissinger plots for the calculation of the activation energies of a) the all the coatings and b) the mixture of NC547 and PDMS.

The lower E_a values of samples cured with FA in relation with those cured with DAPM can be explained in terms of steric hindrance. FA has an amino group that is not sterically hindered (which enables it to react freely). In contrast, DAPM has two amino groups in which both are two carbon-carbon bonds apart from the methyl groups. Thus, DAPM is highly hindered by the presence of the methyl groups. This difference in steric hindrance is the reason that FA showed a lower E_a in comparison with that of DAPM.

Moreover, the incorporation of PDMS did not change the E_a values of the samples with the same kind of curing agent. This suggests that the curing agent was the main component that participated in the reaction with the epoxy groups. In addition, this result showed that PDMS

acted as plasticizer that promoted the reaction between the epoxy and amino groups as seen in the increment of the epoxy conversion.

However, the E_a value increased in the sample NC547-DAPM-PDMS, which indicates that PDMS has participated in the reaction with epoxy groups in this exceptional case. This reaction may have happened through the available amino groups at the end of the siloxane chain. In order to prove this hypothesis, NC547 was mixed with PDMS in a stoichiometry molar ratio and the energy activation was calculated from the Kissinger plot (Figure 4b). The E_a of NC547-PDMS was 100.77 kJ/mol, which is much higher than that of NC547-DAPM (45.41 kJ/mol). The higher E_a of the reaction of PDMS and NC547 was attributed to the obstruction of the long siloxane chains that have prevented the encounter of the amino and epoxy groups. Therefore, since the reaction between PDMS and NC547 was energetically costly, the increment in the energy of activation of NC547-DAPM caused by the addition of PDMS was because that PDMS also links with the epoxy resin. As a consequence, PDMS not only acts as plasticizer in NC547-DAPM-PDMS but also as a curing agent. Finally, despite the different activation energies of the six samples, the results suggest that viscosity was the main factor that govern the degree of the epoxy conversion. The 5.5 hours curing time was long enough to suppress the differences in the activation energies, and the final epoxy conversion was the result of the viscosity of the mixture.

Wettability

The wettability properties of the coatings were assessed by measuring the water contact angles (WCA) and surface energy (Table 1). In the absence of PDMS, all the samples were hydrophilic (WCA < 90°) with the exception of NC514-DAPM (WCA= 95.43°). This result can be explained by the percentage of epoxy conversion. The hydrophilicity of NC547-FA

and NC547-DAPM is due to the moderate concentration of the remaining epoxy groups which can form hydrogen bonds with water. In contrast, NC514-DAPM was slightly hydrophobic due to adequate exposure of the long carbon chains without the chemical interference of unreacted epoxy groups. The same argument can be used for the explanation of the surface energy of the PDMS-free coatings, where NC514-DAPM has the lowest surface energy among the three coatings. On the other hand, the incorporation of PDMS has caused the coatings to become hydrophobic (WCA > 90°) for all the NC547-based coatings. Although epoxy groups still remained in the cured samples, the concentration of PDMS was high enough to overcome the hydrophilic properties of the unreacted epoxy groups. In case of the NC514-based samples, the addition of PDMS into NC514-DAPM caused the coating to show a higher WCA (from 95.43° to 114.00°). This is a consequence of the increment of the methyl groups of PDMS on the surface of the coating. The high concentration of PDMS on the surface of NC514-DAPM-PDMS can be proved by its FTIR spectrum that resembled that of PDMS (Figure 2d). This result suggests that certain amount of PDMS was present on the coating surface. In all the cases, addition of PDMS was accompanied by the decrease of the surface energy of the coatings (Table 1).

Thermal and mechanical properties

The thermal properties of the bio-based coatings were studied by TGA (Figure 5). The onset temperature of decomposition (T_d) and amount of residue of the samples are shown in Table 2. The T_d and the residue percentages of the coatings without PDMS decreased in the following order: NC547-FA > NC547-DAPM > NC514-DAPM. In case of samples based on NC547, the result suggested that FA provided better thermal resistance than that of DAPM. This can be supported by the fact that aromatic compounds like FA are well known by their

high thermal resistance in comparison with non-aromatic compounds such as DAPM [46]. However, despite the better thermal resistance showed by FA in comparison with DAPM in the beginning of the pyrolysis, the residue percentages of NC547-FA (11.19%) and NC547-DAPM (10.74%) were quite similar. This is because the curing agents (FA and DAPM) were mostly decomposed in the form of gases and the epoxy resin (NC547) remained as the major component of the char. On the other hand, the effect of epoxy resin can be studied from the T_d of NC547-DAPM and NC514-DAPM. The slight difference in the T_d of NC547-DAPM (254.76 °C) and NC514-DAPM (247.57 °C) demonstrates that NC514 was slightly less resistant than NC547. Nevertheless, a considerable difference in the residues between NC547-DAPM (10.74 %) and NC514-DAPM (5.39 %) was noticed. This indicates that most of the mass of NC514 was decomposed in the form of gases, which can be attributed to the lower concentration of benzene rings of N514 (two benzene rings per molecule) in comparison with that of N547 (five benzene rings per molecule).

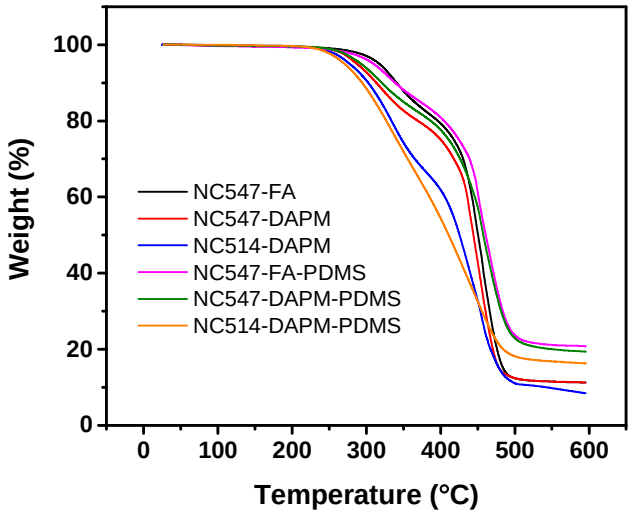

Figure 5. TGA thermographs of the epoxy cardanol-based coatings.

With the incorporation of PDMS, the T_d values of the samples followed the same order as the ones without PDMS (NC547-FA-PDMS > NC547-DAPM-PDMS > NC514-DAPM-PDMS), and all of them were lower than their PDMS-free counterparts. Therefore, the reduction of the T_d values can be attributed to the early decomposition of PDMS. In addition, the T_d results also demonstrate that FA imparted a better thermal resistance than DAPM in the beginning of the pyrolysis. Moreover, the lower T_d value of NC514-DAPM-PDMS (224.38°C) in relation to that of NC547-DAPM-PDMS (243.21°C) clearly shows that NC514 was less thermally resistant than NC547.

Although PDMS started to decompose early, much of the mass of PDMS in its decomposed form remained after burning, and has increased the residue percentages. The residues of NC547-FA-PDMS (20.93%) and NC547-DAPM-PDMS (20.07%) were quite similar and supported the mechanism in which FA and DAPM decomposed firstly and the residues mainly originated from the NC547 and PDMS. Moreover, the lower residue percentage of NC514-DAPM-PDMS (15.63 %) in comparison with NC547-DAPM-PDMS (20.07%) proves once again that NC514 degraded mainly in the form of volatile gases.

Table 2. Thermal and mechanical properties of the bio-based samples.

Sample	T_d (°C)	Residue (%)	T_g (°C)	v_e (mol/m^3)
NC547-FA	288 (±1)	11 (±0)	31 (±2)	25 (±3)
NC547-DAPM	255 (±3)	11 (±1)	46 (±4)	24 (±4)
NC514-DAPM	248 (±3)	5 (±0)	46 (±0)	45 (±1)
NC547-FA-PDMS	275 (±2)	21 (±1)	30 (±1)	30 (±3)
NC547-DAPM-PDMS	243 (±3)	20 (±2)	41 (±2)	28 (±4)
NC514-DAPM-PDMS	224 (±2)	16 (±2)	44 (±1)	36 (±2)

DMA was carried out to measure the glass transition and crosslink density of the bio-based thermosets (Table 2). The glass transition (T_g) of the coatings was measured as the temperature corresponding to the peak of the Tanδ ($T_{Tan\delta}$). The crosslink densities (v_e) of the thermosets were measured according to the following equation:

$$v_e = \frac{E}{3RT} \qquad (3)$$

where E is the storage modulus at the temperature T (T = 30°K + $T_{Tan\delta}$) and R is the universal gas constant [47]. The T_g values of the samples without PDMS showed a dependency on the type of bio-based curing agent rather than on the type of epoxy resin. That is, the samples cured with DAPM (NC547-DAPM and NC514-DAPM) had very similar T_g values (~46 °C), while the sample cured with FA had a lower T_g (31.28 °C). The difference in the T_g was ascribed to the size and branched nature of the curing agents. Apart from being a molecule bigger than FA, DAPM is a dynamic molecule that undergoes conformations and has bulkier CH_3- groups that can prevent the movement of the polymer network more effectively than FA, and thus, the increase in the T_g. On the other hand, the incorporation of PDMS slightly decreased the T_g values due to the flexible nature of PDMS that has softened the polymer network.

The crosslink density values (v_e) of bio-based coatings were also analyzed. Among the samples without PDMS, the v_e values of NC547-FA and NC547-DAPM were similar (~24 mol/m^3), and lower than that of NC514-DAPM (44.60 mol/m^3). The low and similar v_e values of NC547-FA and NC547-DAPM can be explained by the low and similar degree of epoxy conversion (Table 1). Similarly, the NC514-DAPM exhibited a higher v_e as the result of the complete conversion of epoxy groups. After the incorporation of PDMS, v_e of the

NC514-based samples decreased. This decrease in v_e can be attributed to the hindrance caused by the diffusion of PDMS to the surface during curing. That is, although PDMS did not affect the degree of curing, its migration to the surface might have reduced the closeness of the crosslink points, and therefore, decreased the crosslink density. On the other hand, the effect of PDMS on the v_e values of NC547-based coatings was not clear due to their similar v_e values. Nevertheless, if the measured v_e of PDMS-NC547 samples are considered significant, it is possible to indicate that NC547-based coatings showed slightly high v_e value with the addition of PDMS. Then, the slight increment in v_e of NC547-based coatings can be explained by the higher degree of curing that has yielded an increased number of chemical bonds.

In addition of their higher v_e values, NC514-based samples also showed higher Tanδ peaks than NC547-based samples (Figure S2). The high Tanδ peaks of the NC514-based polymers means that the coatings have a higher degree of viscous behavior than those of the NC547-based polymers. This result can be explained in terms of the rigidity of the molecular structure of the bio-epoxies. NC514 is more flexible due to the presence of two separated benzene rings per molecule while NC547 is more rigid due to its five consecutive benzene groups per molecule.

Anti-icing performance

The potential use of the coatings as protection against the formation of ice on the surface was evaluated by measuring the ice adhesion strengths (Figure 6, Table 3). The results show that all the coatings had a low affinity to the ice in comparison with the bare iron substrate. Moreover, the coatings with PDMS showed a further lower ice adhesion strength than the coatings without PDMS. Most researchers in the community have accepted the suggestion

that coatings with ice adhesion strength lower than 100 kPa can be considered as icephobic [48]. Based on this definition, the bio-based coatings are icephobic since the average ice adhesion strength of all the coatings was about 50 kPa. However, there are other suggestions that icephobic coatings for real applications should have ice adhesion strengths lower than 10 kPa[49]. As discussed recently, it is not possible to have a fair comparison among the ice adhesion test results reported in the literature due to the lack of a standard protocol[49, 50]. Different testing methods have been used under different sample and facility conditions. Thus, the ice adhesion strengths of the bio-based coatings obtained in this study can be best compared with coatings reported using the same ice-adhesion set up and conditions. The ice adhesion strengths of the new bio-based films were better than the superhydrophobic isosorbide-based coatings that exhibited ice adhesion strengths around 100 kPa[22], and comparable to the hydrophobic bio-epoxy coatings with ice adhesion strengths around 50 kPa[26].

According to literature, various factors affect the ice adhesion of the coatings such as surface topology, roughness, surface energy and wettability [51-53]. Therefore, the anti-icing performances of the coatings were evaluated by comparing the surface properties (Table 3).

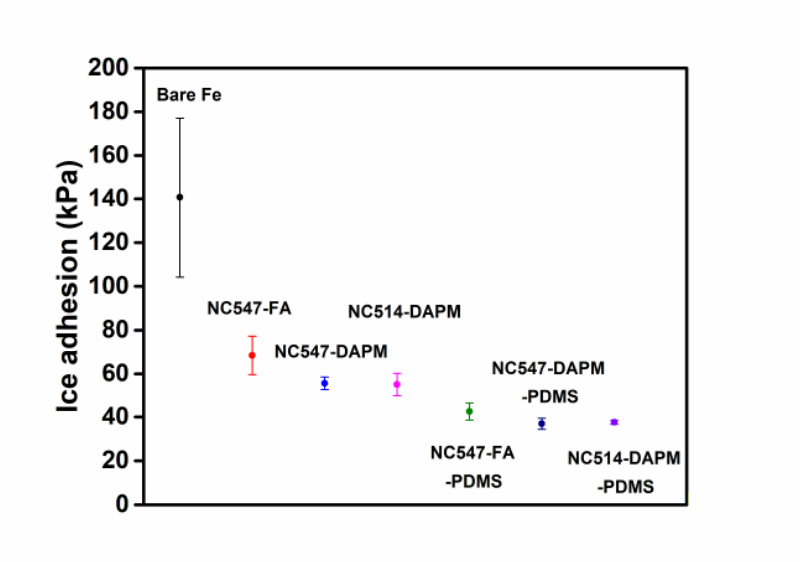

Figure 6. Comparison of ice adhesion strength of the bio-based coatings.

The roughness of the coatings was assessed as the root mean square (RMS) of the heights of the surfaces. The results show that all coatings are very smooth with RMS largely below 30 nm. With such a small roughness, the actual surface area is close to the nominal area. As reported in the literature, properly designed surface topology with a high roughness in the range of hundreds of nanometers might be suitable for anti-icing application as it can trap much air on the surface structure [38, 54]. However, this mechanism is not operative in the ultra-smooth coatings in the current work.

The lower ice adhesion strengths in the current work come from the lower surface energy in comparison with the bare substrate. The WCAs of the coatings were higher than that of the iron substrate (WCA=59.31 ± 0.77°). Similarly, the better anti-icing performances of the PDMS-containing coatings in relation with PDMS-free samples were ascribed to their higher WCAs and lower surface energies (Table 1) [55]. It is worth mentioning that although NC514-DAPM was hydrophobic (WCA=95.43°) before the incorporation of PDMS, its surface

energy was not low enough to exhibit an ice adhesion strength value similar to those of the PDMS-containing samples.

Contact angle hysteresis may have an influence on the anti-icing performances of the coatings [56, 57]. Therefore, the water contact angle hysteresis data of the coatings were also assessed (Table 3). The contact angle hysteresis ($\theta_A - \theta_R$) of samples without PDMS were higher than the samples with PDMS. This reveals that water affinity was higher on the surfaces of coatings without PDMS. Moreover, the contact angle hysteresis in each series of samples (coatings with/without PDMS) did not vary as significantly as in the surface energy measurements (Table 1). Thus, apart from the surface energy properties, the contact angle hysteresis may serve as an indicator of the ice adhesion strengths. Surfaces with low WCA hysteresis has a better ability to repel water, therefore low ice adhesion strengths are expected on this type of smooth surface.

The reduction of the contact angle hysteresis caused by PDMS can be attributed to its liquid-like and smooth surface at the molecular level [58]. A liquid-like surface is unable to hold a liquid firmly and, therefore, causing the liquid to slide. The liquid-like surface of PDMS can be attributed to the arrangement of methyl groups along the siloxane chain. The methyl groups in PDMS are separated from each other by an oxygen bridge that can be considered as a molecular spacer[59]. This molecular space allows the methyl groups to have a free movement that causes the formation of an unstable surface (liquid-like surface). Contrarily, in the hypothetical case of the absence of the oxygen bridges, methyl groups would pack better and, as a consequence, a more rigid molecular surface would form. In addition of its liquid-like surface, PDMS also has a smooth molecular surface that relies on the uniformity of the branches in the siloxane chain. The methyl groups constitute the main branches of the

siloxane chain and therefore, it creates a smooth surface that reduces the hysteresis. In case of PDMS having different kinds of branches such as alternating methyl and octyl groups, the surface would be rough at the molecular level and probably exhibiting a higher hysteresis. The positive effect PDMS on anti-icing properties resembles that of the slippery liquid-infused porous surfaces (SLIPS) [60], which consists of porous surfaces impregnated with an immiscible liquid. The low hysteresis of SLIPS comes from the thin hydrophobic liquid layer that offers a defect-free and smooth surface at the molecular level [61, 62].

Table 3. Ice adhesion values, RMS and θ_A and θ_R of water droplets.

Sample	Ice adhesion strength (kPa)	RMS (nm)	θ_A (°)	θ_R (°)	θ_A-θ_R (°)
Fe substrate	140.7 (± 36.4)	-	-	-	-
NC547-FA	68.5 (± 8.8)	8.61 (± 1.33)	83.16 (± 0.97)	46.33 (± 0.93)	36.83
NC547-DAPM	55.6 (± 2.9)	19.62 (± 1.95)	86.56 (± 0.67)	51.54 (± 1.18)	35.02
NC514-DAPM	55.0 (± 5.2)	8.51 (± 2.58)	107.59 (± 0.31)	72.39 (± 0.59)	35.2
NC547-FA-PDMS	42.6 (± 4.0)	27.91 (± 10.02)	104.92 (± 0.81)	77.46 (± 1.34)	27.46
NC547-DAPM-PDMS	36.9 (± 2.6)	31.50 (± 6.62)	102.95 (± 0.91)	71.48 (± 1.03)	31.47
NC514-DAPM-PDMS	37.6 (± 0.9)	*	117.21 (± 0.45)	85.85 (± 0.33)	31.36

* It was not possible to measure the roughness of NC514-DAPM-PDMS due to its soft surface that prevented the AFM scanning.

Anticorrosion performance

The anticorrosion performance of the thin samples was assessed by calculating the corrosion potential (E_{corr}) and corrosion current (I_{corr}) from the Tafel curves (Figure 7). The Tafel curves of the coatings shifted to higher potentials (E_{corr}) and lower current densities (I_{corr}) in comparison with the unprotected Fe substrate (Table 4). It is clear that all coatings (with or without PDMS) are able to improve the corrosion resistance of the Fe substrate, as evidenced by the much positive corrosion potentials and the ~2 orders of magnitude reduction in the corrosion current densities. However, due to the varying viscosity, it was difficult to prepare

coatings with the same thickness for a better comparison, since the E_{corr} and I_{corr} values can be affected by the coating thicknesses.

The anticorrosion performance of the coatings can be analyzed from the point of view of crosslink density and hydrophobicity. A high crosslink-density coating is generally characterized by a reduced free volume of the polymer network that can block the diffusion of the electrolyte better than a low crosslink-density coating [63]. Similarly, hydrophobic surfaces are expected to have a better corrosion protection than hydrophilic surfaces because of their low affinity with water [64]. The E_{corr} and I_{corr} values of the samples without PDMS showed that NC514-DAPM and N547-DAPM had better anticorrosion properties than NC547-FA. The higher E_{corr} value and low I_{corr} value of NC514-DAPM, despite its thinner thickness, can be ascribed to its high crosslink density as well as its inherent hydrophobicity.

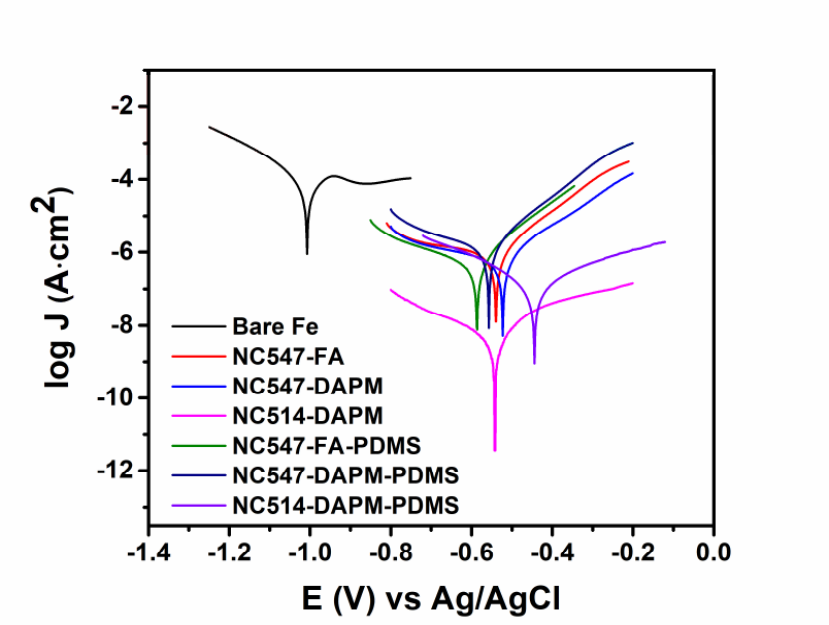

Figure 7. Typical Tafel curves of the bio-based coatings.

Nonetheless, the explanation of the high E_{corr} value and lowest I_{corr} value of NC547-FA was not clear since the coating exhibited a low crosslink density and hydrophilicity. Therefore, it is possible that the good anticorrosive properties of NC547-FA were caused by its higher thickness. In case of NC547-DAPM, its low anticorrosion performance could be attributed to its low crosslink density and hydrophilicity. Thus, corrosion data of the samples without PDMS suggest that high E_{corr} and low I_{corr} values were obtained when the coatings had higher crosslink density and hydrophobicity.

There is a difficulty in thoroughly analyzing the influence of PDMS addition on the anticorrosion performance because of different thicknesses obtained in this study. Nevertheless, two pairs of coatings with similar thickness were compared. The first pair was between NC514-DAPM (2.98 µm) and NC547-DAPM-PDMS (2.72 µm), and both were hydrophobic. The hydrophocity of NC514-DAPM came from the surface exposure of the long carbon chains while their hydrophobicity of NC547-DAPM-PDMS was caused by siloxane chains of PDMS. Despite the fact that both of them are hydrophobic, the anticorrosion performance of the coatings was different. NC514-DAPM had a higher E_{corr} and lower I_{corr} than those of NC547-DAPM-PDMS. The difference in performance can be ascribed to the different crosslink densities. As analyzed above, NC547-DAPM-PDMS did not cure completely while NC514-DAPM did. Therefore, when hydrophobicity condition is achieved in the coatings, crosslink density becomes an important factor on the anticorrosive properties of the coatings. The second pair for comparison was NC547-FA-PDMS (7.28 µm) and NC514-DAPM-PDMS (7.57 µm). Both were hydrophobic due to the presence of PDMS but they showed different anticorrosion performance. NC514-DAPM-PDMS demonstrated a better protection against corrosion than NC547-FA-PDMS. Since both of them were

hydrophobic, the crosslink density difference seemed to be the most reasonable explanation for the different anticorrosion performances. As showed in Table 2, NC514-DAPM-PDMS had higher v_e value (35.95 mol/cm^3) than that of NC547-FA-PDMS (29.89 mol/cm^3). This suggests again the anticorrosive properties of the hydrophobic coatings are affected by the crosslink density. These results are similar to other recent results in which the importance of balancing the hydrophobicity and crosslink density (barrier properties) of coatings was highlighted [65-68].

Table 4. Corrosion data together with thickness values.

Sample	Thickness (µm)	E_{corr} (V vs Ag/AgCl)	log (I_{corr} (A/cm^2))	I_{corr} (A/cm^2) x 10^{-7}
Fe substrate	-	- 1.00 (±0.01)	-4.10 (± 0.11)	820 (± 231)
NC547-FA	9.13 (±3.89)	-0.49 (±0.05)	-7.88 (±1.64)	3.4 (± 5.58)
NC547-DAPM	4.54 (±0.65)	-0.54 (±0.04)	-6.28 (± 0.29)	11.13 (± 14.11)
NC514-DAPM	2.98 (±1.17)	-0.49 (±0.09)	-6.72 (±1.48)	5.85 (± 3.05)
NC547-FA-PDMS	7.28 (±2.90)	-0.53 (±0.05)	-6.25 (±0.20)	6.08 (± 3.03)
NC547-DAPM-PDMS	2.72 (±0.73)	-0.57 (±0.02)	-5.76 (±0.20)	18.80 (± 9.77)
NC514-DAPM-PDMS	7.57 (±4.60)	-0.48 (±0.05)	-6.95 (±0.03)	1.12 (± 0.07)

CONCLUSIONS

The use of FA and DAPM as curing agents was explored in the preparation of new thermosets coatings from bio-based cardanol-derived epoxy resins NC547 and NC514. The coatings were also hydrophobized by incorporating PDMS, and their anti-icing and anticorrosion properties were evaluated. Due to its low viscosity, NC514-based coatings exhibited a complete consumption of the epoxy groups while the NC547-based coatings could not achieve a full consumption, due to its higher viscocity. Samples became more hydrophobic with the addition of PDMS. Both series of coatings (with and without addition of PDMS)

displayed sufficiently low ice adhesion strength (< 100 kPa), which makes them good candidates for icephobic applications. The addition of PDMS has resulted in a further reduction of the ice adhesion. The incorporation of PDMS might have mixed effects on the anticorrosion performance. On the one hand, the increased hydrophobicity favors the enhanced anticorrosion performance. On the other hand, this enhancement may be compromised if the crosslink density of the coating remains low. Future clarification should be carried out with a better-controlled thickness in the coatings. Finally, due to its inherent hydrophobicity and fully bio-based content, NC514-DAPM is a promising solvent-free coating formulation for anticorrosion and anti-icing applications. NC514-DAPM demonstrated a low ice-adhesion strength at 55.0 ± 5.2 kPa, and when coated on a Fe substrate with a thickness of 3 μm, the corrosion potential was shifted positively by 0.51V, and the corrosion current density was reduced by 2 orders of magnitude.

ASSOCIATED CONTENT

Supporting information

The following files are available free of charge.

Additional figures (PDF).

AUTHOR INFORMATION

Corresponding author

*E-mail: ASZChen@ntu.edu.sg; Tel: +65-67904256; Fax: +65-67909081

Author contributions

The manuscript was written through contributions of all authors. All authors have given approval to the final version of the manuscript

Notes

The authors declare no competing financial interest.

ACKNOWLEDGMENT

We would like to thank the Agency for Science, Technology and Research (A*STAR) of Singapore for the funds (SERC 1528000048) provided in this research.

REFERENCES

1. Ng, F.; Couture, G.; Philippe, C.; Boutevin, B.; Caillol, S. Bio-Based Aromatic Epoxy Monomers for Thermoset Materials. *Molecules* **2017,** *22* (1), 149, DOI 10.3390/molecules22010149.
2. Jin, F.-L.; Li, X.; Park, S.-J. Synthesis and application of epoxy resins: A review. *Journal of Industrial and Engineering Chemistry* **2015,** *29*, 1-11, DOI 10.1016/j.jiec.2015.03.026.
3. Samal, S. K.; Mohanty, S.; Nayak, S. K. Recent Development of Biobased Epoxy Resins: A Review. *Polymer-Plastics Technology and Engineering* **2018,** *57* (3), 133-155, DOI 10.1080/03602559.2016.1253742.
4. Kumar, S.; Krishnan, S.; Mohanty, S.; Nayak, S. K. Synthesis and characterization of petroleum and biobased epoxy resins: a review. *Polymer International* **2018,** *67* (7), 815-839, DOI 10.1002/pi.5575.
5. Çayli, G.; Gürbüz, D.; Çınarli, A. Characterization and Polymerization of Epoxidized Methacrylated Castor Oil. *European Journal of Lipid Science and Technology* **2019,** *121* (1), 1700189, DOI 10.1002/ejlt.201700189.
6. Sahoo, S. K.; Khandelwal, V.; Manik, G. Development of completely bio-based epoxy networks derived from epoxidized linseed and castor oil cured with citric acid. *Polymers for Advanced Technologies* **2018,** *29* (7), 2080-2090, DOI 10.1002/pat.4316.
7. Chang, R.; Qin, J.; Gao, J. RETRACTED ARTICLE: Fully biobased epoxy from isosorbidediglycidyl ether cured by biobased curing agents with enhanced properties. *Journal of Polymer Research* **2014,** *21* (7), 501, DOI 10.1007/s10965-014-0501-9.
8. Marotta, A.; Ambrogi, V.; Cerruti, P.; Mija, A. Green approaches in the synthesis of furan-based diepoxy monomers. *RSC Advances* **2018,** *8* (29), 16330-16335, DOI 10.1039/C8RA02739K.
9. Janvier, M.; Hollande, L.; Jaufurally, A. S.; Pernes, M.; Ménard, R.; Grimaldi, M.; Beaugrand, J.; Balaguer, P.; Ducrot, P.-H.; Allais, F. Syringaresinol: A Renewable and Safer Alternative to Bisphenol A for Epoxy-Amine Resins. *ChemSusChem* **2017,** *10* (4), 738-746, DOI 10.1002/cssc.201601595.
10. Shang, L.; Zhang, X.; Zhang, M.; Jin, L.; Liu, L.; Xiao, L.; Li, M.; Ao, Y. A highly active bio-based epoxy resin with multi-functional group: synthesis, characterization, curing and properties. *Journal of Materials Science* **2018,** *53* (7), 5402-5417, DOI 10.1007/s10853-017-1797-8.
11. Thachil, E. T. Synthesis and Characterization of Cardanol-Based Epoxy Systems. *Designed Monomers and Polymers* **2008,** *11* (6), 593-607, DOI 10.1163/156855508X363870.
12. Jaillet, F.; Darroman, E.; Ratsimihety, A.; Auvergne, R.; Boutevin, B.; Caillol, S. New biobased epoxy materials from cardanol. *European Journal of Lipid Science and Technology* **2014,** *116* (1), 63-73, DOI 10.1002/ejlt.201300193.

13. Kanehashi, S.; Yokoyama, K.; Masuda, R.; Kidesaki, T.; Nagai, K.; Miyakoshi, T. Preparation and characterization of cardanol-based epoxy resin for coating at room temperature curing. *Journal of Applied Polymer Science* **2013,** *130* (4), 2468-2478, DOI 10.1002/app.39382.
14. Darroman, E.; Durand, N.; Boutevin, B.; Caillol, S. New cardanol/sucrose epoxy blends for biobased coatings. *Progress in Organic Coatings* **2015,** *83*, 47-54, DOI 10.1016/j.porgcoat.2015.02.002.
15. Darroman, E.; Durand, N.; Boutevin, B.; Caillol, S. Improved cardanol derived epoxy coatings. *Progress in Organic Coatings* **2016,** *91*, 9-16, DOI 10.1016/j.porgcoat.2015.11.012.
16. Gour, R. S.; Raut, K. G.; Badiger, M. V. Flexible epoxy novolac coatings: Use of cardanol-based flexibilizers. *Journal of Applied Polymer Science* **2017,** *134* (23), 1-12, DOI 10.1002/app.44920.
17. Gour, R. S.; Kodgire, V. V.; Badiger, M. V. Toughening of epoxy novolac resin using cardanol based flexibilizers. *Journal of Applied Polymer Science* **2016,** *133* (16), 1-9, DOI 10.1002/app.43318.
18. Natarajan, M.; Murugavel, S. C. Cure kinetics of bio-based epoxy resin developed from epoxidized cardanol–formaldehyde and diglycidyl ether of bisphenol–A networks. *Journal of Thermal Analysis and Calorimetry* **2016,** *125* (1), 387-396, DOI 10.1007/s10973-016-5417-7.
19. Nguyen, T. K. L.; Livi, S.; Soares, B. G.; Barra, G. M. O.; Gérard, J.-F.; Duchet-Rumeau, J. Development of Sustainable Thermosets from Cardanol-based Epoxy Prepolymer and Ionic Liquids. *ACS Sustainable Chemistry & Engineering* **2017,** *5* (9), 8429-8438, DOI 10.1021/acssuschemeng.7b02292.
20. Aggarwal, L. K.; Thapliyal, P. C.; Karade, S. R. Anticorrosive properties of the epoxy–cardanol resin based paints. *Progress in Organic Coatings* **2007,** *59* (1), 76-80, DOI 10.1016/j.porgcoat.2007.01.010.
21. Kathalewar, M.; Sabnis, A. Epoxy resin from cardanol as partial replacement of bisphenol-A-based epoxy for coating application. *Journal of Coatings Technology and Research* **2014,** *11* (4), 601-618, DOI 10.1007/s11998-014-9570-2.
22. Zheng, S.; Bellido-Aguilar, D. A.; Wu, X.; Zhan, X.; Huang, Y.; Zeng, X.; Zhang, Q.; Chen, Z. Durable Waterborne Hydrophobic Bio-Epoxy Coating with Improved Anti-Icing and Self-Cleaning Performance. *ACS Sustainable Chemistry & Engineering* **2019,** *7* (1), 641-649, DOI 10.1021/acssuschemeng.8b04203.
23. Bellido-Aguilar, D. A.; Zheng, S.; Zhan, X.; Huang, Y.; Zhao, X.; Zeng, X.; Pallathadka, P. K.; Zhang, Q.; Chen, Z. Effect of a fluoroalkyl-functional curing agent on the wettability, thermal and mechanical properties of hydrophobic biobased epoxy coatings. *Surface and Coatings Technology* **2019,** *362*, 274-281, DOI 10.1016/j.surfcoat.2019.02.006.
24. Zheng, S.; Bellido-Aguilar, D. A.; Huang, Y.; Zeng, X.; Zhang, Q.; Chen, Z. Mechanically robust hydrophobic bio-based epoxy coatings for anti-corrosion application. *Surface and Coatings Technology* **2019,** *363*, 43-50, DOI 10.1016/j.surfcoat.2019.02.020.
25. Zheng, S.; Bellido-Aguilar, D. A.; Hu, J.; Huang, Y.; Zhao, X.; Wang, Z.; Zeng, X.; Zhang, Q.; Chen, Z. Waterborne bio-based epoxy coatings for the corrosion protection of metallic substrates. *Progress in Organic Coatings* **2019**, 105265, DOI 10.1016/j.porgcoat.2019.105265.
26. Wu, X.; Zheng, S.; Bellido-Aguilar, D. A.; Silberschmidt, V. V.; Chen, Z. Transparent icephobic coatings using bio-based epoxy resin. *Materials & Design* **2018,** *140*, 516-523, DOI 10.1016/j.matdes.2017.12.017.
27. Liu, C.; Liu, Z.; Tisserat, B. H.; Wang, R.; Schuman, T. P.; Zhou, Y.; Hu, L. Microwave-assisted maleation of tung oil for bio-based products with versatile applications. *Industrial Crops and Products* **2015,** *71*, 185-196, DOI 10.1016/j.indcrop.2015.02.066.
28. Jiang, H.; Sun, L.; Zhang, Y.; Liu, Q.; Ru, C.; Zhang, W.; Zhao, C. Novel biobased epoxy resin thermosets derived from eugenol and vanillin. *Polymer Degradation and Stability* **2019,** *160*, 45-52, DOI 10.1016/j.polymdegradstab.2018.12.007.

29. Karami, Z.; Nademi, F.; Zohuriaan-Mehr, M. J.; Rostami, A. An efficient fully bio-based reactive diluent for epoxy thermosets: 2-[(Oxiran-2-ylmethoxy) methyl] furan versus a petroleum-based counterpart. *Journal of Applied Polymer Science* **2017,** *134* (25), 1-9, DOI 10.1002/app.44957.
30. He, X.; Conner, A. H.; Koutsky, J. A. Evaluation of furfurylamines as curing agents for epoxy resins. *Journal of Polymer Science Part A: Polymer Chemistry* **1992,** *30* (4), 533-542, DOI 10.1002/pola.1992.080300403.
31. Gnanapragasam, S.; Krishnan, S.; Arumugam, H.; Chavali, M.; Alagar, M. Synthesis and characterization of a novel high-performance benzoxazine from benzaldehyde-based bisphenol. *Advances in Polymer Technology* **2018,** *37* (8), 3056-3065, DOI 10.1002/adv.21976.
32. Viet, C. X.; Lan, D. N. U.; Hung, T. K. Thermal Curing of Benzoxazine Blends from Cardanol-Furfurylamine and Diphenolic Acid-Aniline. *IOP Conference Series: Materials Science and Engineering* **2018,** *429*, 012068, DOI 10.1088/1757-899x/429/1/012068.
33. Shen, X.; Dai, J.; Liu, Y.; Liu, X.; Zhu, J. Synthesis of high performance polybenzoxazine networks from bio-based furfurylamine: Furan vs benzene ring. *Polymer* **2017,** *122*, 258-269, DOI 10.1016/j.polymer.2017.06.075.
34. Wang, C.; Zhao, C.; Sun, J.; Huang, S.; Liu, X.; Endo, T. Synthesis and thermal properties of a bio-based polybenzoxazine with curing promoter. *Journal of Polymer Science Part A: Polymer Chemistry* **2013,** *51* (9), 2016-2023, DOI 10.1002/pola.26587.
35. Trumbo, D. L. Synthesis of polyamides based on 1,8-diamino-p-menthane. *Journal of Polymer Science Part A: Polymer Chemistry* **1988,** *26* (10), 2859-2862, DOI 10.1002/pola.1988.080261023.
36. Donnellan, T.; Roylance, D. The curing of a bisphenol A-type epoxy resin with 1,8 diamino-p-menthane. *Polymer Engineering & Science* **1982,** *22* (13), 821-825, DOI 10.1002/pen.760221306.
37. Moy, E.; Neumann, A. W. Solid/liquid interfacial tensions from contact angle data and direct force measurements. *Journal of Colloid and Interface Science* **1987,** *119* (1), 296-297, DOI 10.1016/0021-9797(87)90273-6.
38. Fu, Q.; Wu, X.; Kumar, D.; Ho, J. W. C.; Kanhere, P. D.; Srikanth, N.; Liu, E.; Wilson, P.; Chen, Z. Development of Sol–Gel Icephobic Coatings: Effect of Surface Roughness and Surface Energy. *ACS Applied Materials & Interfaces* **2014,** *6* (23), 20685-20692, DOI 10.1021/am504348x.
39. Riehle, N.; Götz, T.; Kandelbauer, A.; Tovar, G. E. M.; Lorenz, G. Data on the synthesis and mechanical characterization of polysiloxane-based urea-elastomers prepared from amino-terminated polydimethylsiloxanes and polydimethyl-methyl-phenyl-siloxane-copolymers. *Data in Brief* **2018,** *18*, 1784-1794, DOI 10.1016/j.dib.2018.04.083.
40. Ernault, E.; Richaud, E.; Fayolle, B. Thermal oxidation of epoxies: Influence of diamine hardener. *Polymer Degradation and Stability* **2016,** *134*, 76-86, DOI 10.1016/j.polymdegradstab.2016.09.030.
41. Escola, M. A.; Moina, C. A.; Niño Gómez, A. C.; Ybarra, G. O. The determination of the degree of cure in epoxy paints by infrared spectroscopy. *Polymer Testing* **2005,** *24* (5), 572-575, DOI 10.1016/j.polymertesting.2005.02.013.
42. Cholake, S.; Mada, M.; Singh, R.; Bai, Y.; Zhao, X.-L.; Rizkalla, S.; Bandyopadhyay, S. Quantitative Analysis of Curing Mechanisms of Epoxy Resin by Mid- and Near- Fourier Transform Infra Red Spectroscopy. *Defence science journal* **2014,** *64*, 10.14429/dsj.64.7326.
43. Wellen, R. M. R.; Canedo, E. L. On the Kissinger equation and the estimate of activation energies for non-isothermal cold crystallization of PET. *Polymer Testing* **2014,** *40*, 33-38, DOI 10.1016/j.polymertesting.2014.08.008.
44. Hu, J.; Shan, J.; Zhao, J.; Tong, Z. Water resistance and curing kinetics of epoxy resins with a novel curing agent of biphenyl-containing amine synthesized by one-pot method. *Thermochimica Acta* **2015,** *606*, 58-65, DOI 10.1016/j.tca.2015.03.011.

45. Qin, J.; Liu, H.; Zhang, P.; Wolcott, M.; Zhang, J. Use of eugenol and rosin as feedstocks for biobased epoxy resins and study of curing and performance properties. *Polymer International* **2014,** *63* (4), 760-765, DOI 10.1002/pi.4588.
46. Gazzotti, S.; Hakkarainen, M.; Adolfsson, K. H.; Ortenzi, M. A.; Farina, H.; Lesma, G.; Silvani, A. One-Pot Synthesis of Sustainable High-Performance Thermoset by Exploiting Eugenol Functionalized 1,3-Dioxolan-4-one. *ACS Sustainable Chemistry & Engineering* **2018,** *6* (11), 15201-15211, DOI 10.1021/acssuschemeng.8b03655.
47. Wan, J.; Gan, B.; Li, C.; Molina-Aldareguia, J.; Kalali, E. N.; Wang, X.; Wang, D.-Y. A sustainable, eugenol-derived epoxy resin with high biobased content, modulus, hardness and low flammability: Synthesis, curing kinetics and structure–property relationship. *Chemical Engineering Journal* **2016,** *284*, 1080-1093, DOI 10.1016/j.cej.2015.09.031.
48. Hejazi, V.; Sobolev, K.; Nosonovsky, M. From superhydrophobicity to icephobicity: forces and interaction analysis. *Scientific Reports* **2013,** *3*, 2194, DOI 10.1038/srep02194.
49. Irajizad, P.; Nazifi, S.; Ghasemi, H. Icephobic surfaces: Definition and figures of merit. *Advances in Colloid and Interface Science* **2019,** *269*, 203-218, DOI 10.1016/j.cis.2019.04.005.
50. Work, A.; Lian, Y. A critical review of the measurement of ice adhesion to solid substrates. *Progress in Aerospace Sciences* **2018,** *98*, 1-26, DOI 10.1016/j.paerosci.2018.03.001.
51. Shen, Y.; Wu, X.; Tao, J.; Zhu, C.; Lai, Y.; Chen, Z. Icephobic materials: Fundamentals, performance evaluation, and applications. *Progress in Materials Science* **2019,** *103*, 509-557, DOI 10.1016/j.pmatsci.2019.03.004.
52. Liu, B.; Zhang, K.; Tao, C.; Zhao, Y.; Li, X.; Zhu, K.; Yuan, X. Strategies for anti-icing: low surface energy or liquid-infused? *RSC Advances* **2016,** *6* (74), 70251-70260, DOI 10.1039/C6RA11383D.
53. Menini, R.; Farzaneh, M. Advanced Icephobic Coatings. *Journal of Adhesion Science & Technology* **2011,** *25* (9), 971-992, DOI 10.1163/016942410X533372.
54. Wu, X.; Silberschmidt, V. V.; Hu, Z.-T.; Chen, Z. When superhydrophobic coatings are icephobic: Role of surface topology. *Surface and Coatings Technology* **2019,** *358*, 207-214, DOI 10.1016/j.surfcoat.2018.11.039.
55. Li, H.; Li, X.; Luo, C.; Zhao, Y.; Yuan, X. Icephobicity of polydimethylsiloxane-b-poly(fluorinated acrylate). *Thin Solid Films* **2014,** *573*, 67-73, DOI 10.1016/j.tsf.2014.11.007.
56. Sarshar, M. A.; Swarctz, C.; Hunter, S.; Simpson, J.; Choi, C.-H. Effects of contact angle hysteresis on ice adhesion and growth on superhydrophobic surfaces under dynamic flow conditions. *Colloid and Polymer Science* **2013,** *291* (2), 427-435, DOI 10.1007/s00396-012-2753-4.
57. Zhuo, Y.; Li, T.; Wang, F.; Håkonsen, V.; Xiao, S.; He, J.; Zhang, Z. An ultra-durable icephobic coating by a molecular pulley. *Soft Matter* **2019,** *15* (17), 3607-3611, DOI 10.1039/C9SM00162J.
58. Fadeev, A. Y.; McCarthy, T. J. Trialkylsilane Monolayers Covalently Attached to Silicon Surfaces: Wettability Studies Indicating that Molecular Topography Contributes to Contact Angle Hysteresis. *Langmuir* **1999,** *15* (11), 3759-3766, DOI 10.1021/la981486o.
59. Hozumi, A.; Urata, C. Development of environmentally-friendly surface modification technology: Practical realization of novel oleophobic coating without relying on perfluorinated compounds and surface texturing. *Synthesiology* **2014,** *7* (3), 190-198, DOI 10.5571/synth.7.190.
60. Wilson, P. W.; Lu, W.; Xu, H.; Kim, P.; Kreder, M. J.; Alvarenga, J.; Aizenberg, J. Inhibition of ice nucleation by slippery liquid-infused porous surfaces (SLIPS). *Physical Chemistry Chemical Physics* **2013,** *15* (2), 581-585, DOI 10.1039/C2CP43586A.
61. Wong, T.-S.; Kang, S. H.; Tang, S. K. Y.; Smythe, E. J.; Hatton, B. D.; Grinthal, A.; Aizenberg, J. Bioinspired self-repairing slippery surfaces with pressure-stable omniphobicity. *Nature* **2011,** *477* (7365), 443-447, DOI 10.1038/nature10447.

62. Kim, P.; Wong, T.-S.; Alvarenga, J.; Kreder, M. J.; Adorno-Martinez, W. E.; Aizenberg, J. Liquid-Infused Nanostructured Surfaces with Extreme Anti-Ice and Anti-Frost Performance. *ACS Nano* **2012,** *6* (8), 6569-6577, DOI 10.1021/nn302310q.
63. Joo, M.; Chiu, T.-M.; Castaneda, H.; Soucek, M. D. Corrosion resistance of alkoxysilane modified bisphenol A-epoxide coatings. *Progress in Organic Coatings* **2019,** *134*, 209-218, DOI 10.1016/j.porgcoat.2019.05.006.
64. Jaramillo, A. F.; Montoya, L. F.; Prabhakar, J. M.; Sanhueza, J. P.; Fernández, K.; Rohwerder, M.; Rojas, D.; Montalba, C.; Melendrez, M. F. Formulation of a multifunctional coating based on polyphenols extracted from the Pine radiata bark and functionalized zinc oxide nanoparticles: Evaluation of hydrophobic and anticorrosive properties. *Progress in Organic Coatings* **2019,** *135*, 191-204, DOI 10.1016/j.porgcoat.2019.06.011.
65. Mihelčič, M.; Slemenik Perše, L.; Šest, E.; Jerman, I.; Giuliani, C.; Di Carlo, G.; Lavorgna, M.; Surca, A. K. Development of solvent- and water-borne fluoropolymer protective coatings for patina-free bronze discs. *Progress in Organic Coatings* **2018,** *125*, 266-278, DOI 10.1016/j.porgcoat.2018.09.014.
66. Eduok, U.; Xu, Z.; Szpunar, J. Fabricating protective silica/PMDS composite films for Mg alloy: Correlating bulk silica reinforcement with barrier performance. *Journal of Non-Crystalline Solids* **2018,** *485*, 47-56, DOI 10.1016/j.jnoncrysol.2018.01.037.
67. Wu, Y.; Guo, P.; Zhao, Y.; Liu, X.; Du, Z. Hydrophobic, transparent waterborne polyurethane-polydimethylsiloxane composites prepared from aqueous sol-gel process and applied in corrosion protection. *Progress in Organic Coatings* **2019,** *127*, 231-238, DOI 10.1016/j.porgcoat.2018.06.002.
68. Dun, Y.; Zhao, X.; Tang, Y.; Dino, S.; Zuo, Y. Microstructure and corrosion resistance of a fluorosilane modified silane-graphene film on 2024 aluminum alloy. *Applied Surface Science* **2018,** *437*, 152-160, DOI 10.1016/j.apsusc.2017.12.109.

SYNOPSIS: Study of the anti-icing and anticorrosion properties of bio-based coatings derived from bio-based epoxy resins and curing agents.